Analysis on Stability Margin of Nb_3Sn Cable-in-Conduit-Conductor

Qiuliang Wang, Cheon Seog Yoon, Keeman Kim
Energy Laboratory, Samsung Advanced Institute of Technology, Taejon 305-380, Korea

Abstract—**The stability margin of Nb_3Sn Cable-in-Conduit Conductor(CICC) has been analyzed by a numerical model. The numerical code is based on the finite volume method to discretize the one-dimensional conservation equations on the staggered mesh. The algebraic method is used to transform the non-uniform mesh in the physical plane to the uniform mesh in the computational plane. The numerical simulation shows that the faster supercritical helium mass flow rate can improve the stability and increase the limiting current. The stability and limiting current are decreased with the increasing the operating temperature and background field. The shorter disturbance duration time allows the higher stability in the well-cooled region and the lower stability in the ill-cooled region.**

Index Terms—Stability Margin; cable-in-Conduit Conductor; staggered mesh; coordinate transformation

I. Introduction

The Korea Superconducting Tokamak Advanced Reactor (KSTAR) is a full superconducting Tokamak with central field of 3.5 T at the radius of 1.8 m [1]. One of important issues in the designing the Tokamak is the stability margin of CICC defined as the maximum input energy that the conductor can absorb and still recover the superconducting state [2]. The stability margin of the CICC strongly depends on the heating induced flow of supercritical helium (SHe). Some experiments showed the mutual coupling of heat transfer and heating induced flow might result in the multi-valued stability margin at zero or lower imposed flow [3]. Generally, the stability margin is limited by the available enthalpy of the SHe. The available enthalpy can be expressed by the function of initial pressure and temperature. In order to study the stability margin of the CICC, a numerical analysis code including the dynamics state equations for the SHe, thermal conduction equations for the strands and conduit has been developed.

II. Numerical Model

In order to simulate the stability margin of the CICC, one–dimensional model is adopted because the longitudinal length of the CICC is relative very longer than its transverse length. The following assumptions are considered to simplify the problem: (1) The thermo-physical properties are uniform over the cross section of the CICC; (2) The effect of current redistribution among strands is relative small; (3) The thermal conductivity of the SHe is ignored because the value is smaller than that of the convection term. The equations for determining the dynamics and thermodynamic state of the SHe are the continuity, momentum and energy conservation equations in conjunction with the thermo-dynamical equations of state. The density, velocity and temperature of the SHe are taken into account as the independent arguments. The one-dimensional equations of the compressible fluid are given as follows [4]:

$$M\frac{\partial \psi}{\partial t} + \Lambda\frac{\partial \psi}{\partial x} = G \tag{1}$$

$$M = \begin{pmatrix} 1 & 0 & 0 \\ 0 & \rho & 0 \\ 0 & 0 & \rho C_v \end{pmatrix},\ \Lambda = \begin{pmatrix} u & \rho & 0 \\ 1/(\rho\alpha) & \rho u & \beta/\alpha \\ 0 & \beta T/\alpha & \rho u C_v \end{pmatrix},$$

$$G = \begin{pmatrix} 0 \\ -f\rho u|u|/(2d_h) \\ (Q_{st} - Q_{cn})/A_{he} + \rho f u^2|u|/(2d_h) \end{pmatrix},\ \psi = \begin{pmatrix} \rho \\ u \\ T \end{pmatrix}$$

where t and x denote the time and space coordinates respectively, α the bulk compressibility coefficient and β the bulk thermal expansion coefficient of SHe, C_V the specific heat of SHe at constant volume, f the friction factor of SHe, d_h the hydraulic diameter, A_{he} the helium cross-sectional area, Q_{st} the heat transfer flux between SHe and strands, Q_{cn} the heat transfer flux between SHe and conduit.

The temperature (T_{st}) of superconducting strands is assumed to be the same in transverse cross-section of the CICC. The temperatures of the strands and the conduit are determined by the thermal conduction equations. Due to a very low thermal conducitvity of stainless steel, the thermal diffusion term in the thermal conduction equation for the conduit is neglected. The thermal conduction equations for the superconducting strands and the conduit are given as follows:

$$\gamma C_{st}\frac{\partial T_{st}}{\partial t} = \frac{\partial}{\partial x}\left(k_{st}\frac{\partial T_{st}}{\partial x}\right) + Q_j + Q_{ij} - \frac{Q_{st} + Q_{st-cd}}{A_{st}} \tag{2}$$

$$\gamma C_{cn}\frac{\partial T_{cn}}{\partial t} = \frac{Q_{cn} + Q_{st-cd}}{A_{cn}} \tag{3}$$

$$Q_{st} = P_{st}h_{he-st}(T_{st} - T)$$

$$Q_{cn} = P_{cd}h_{he-c}(T - T_{cd})$$

$$Q_{st-cd} = P_{st-cd}h_{st-cn}(T_{st} - T_{cd})$$

The manuscript received September 27, 1999.
This work is supported by Korean Ministry of Science and Technology.
Qiuliang Wang's email : qlwang@venus.sait.samsung.co.kr

where γC_{st} is the heat capacity of the strands, γC_{cn} the heat capacity of conduit, k_{st} the thermal conductivity of strands, T_{cn} the temperature of conduit, A_{st} the cross-sectional area of strands, A_{cn} the cross sectional area of conduit, P_{st} the cooling perimeters of strands, P_{cd} cooling perimeter of conduit, $h_{he\text{-}st}$ the heat transfer coefficient between SHe and strands, $h_{he\text{-}c}$ the heat transfer coefficient between SHe and conduit and $h_{st\text{-}cn}$ the heat transfer coefficient between the strands and conduit, Q_j the Joule heating power. The $Q_{st\text{-}cd}$ is used to take into account the possibility for direct heat exchange between the strands and conduit. The contact perimeter between the strands and jacket $P_{st\text{-}cd}$ is of order 50 % of inner conduit perimeter [5]. The external thermal disturbance Q_d can be expressed by a Gaussian function.

The heat transfer coefficient h includes three components, i.e. the transient heat transfer coefficient h_t, Kapitza conductance and steady state heat transfer coefficient h_s. The h_s can be estimated by the Giarratano correction:

$$h_s = \max\left(0.0259\frac{k_{he}}{d_h}Re^{0.8}\,Pr^{0.4}\left(\frac{T}{T_{st}}\right)^{0.716},\frac{8.235k_{he}}{d_h}\right) \quad (4)$$

where k_{he} is the thermal conductivity of SHe, Re the Reynolds number and Pr the Prandtl number. The transient heat transfer coefficient is responsible for the heat coupling between the SHe and the strands at the initial time of the disturbance. The heat transfer coefficient h_t depends on the heat flux $q(t)$. If a disturbance starts at $t = 0$, the h_t and h_k are [6]:

$$h_t = \frac{\sqrt{\pi k_{he}\rho C_p}\,q(t)}{\int_0^t q(t-\tau)\frac{d\tau}{\sqrt{\tau}}} \text{ and } h_k = 200\left(T^2 + T_{st}^2\right)\left(T + T_{st}\right) \quad (5)$$

The heat transfer coefficient between the strands and conduit is calculated by an equivalent heat resistance on the contact surface of strands and conduit.

The total heat transfer coefficient $h_{he\text{-}st}$ between the superconducting strands and the SHe can be expressed as

$$h_{he-st} = \begin{cases} h_k & (t=0) \\ \max\left[\dfrac{h_s h_k}{h_s + h_k}, \dfrac{h_t h_k}{h_t + h_k}\right] & (t>0) \end{cases} \quad (6)$$

The equations (1), (2) and (3) can be solved by the numerical methods combined with the initial and boundary conditions. However, due to the strong heat coupling between the SHe and superconducting strands, the boundary layer located at the normal zone front is very short compared with the length of CICC. In order to obtain a sufficient convergence numerical solution, the interval of space Δx should be so fine that the size is smaller than 1-5 mm [7]. Consequently, a non-uniform mesh should be used for the simulation of stability in a long length CICC. However, the accuracy of solution in the uniform mesh space is much higher than that in the non-uniform mesh space. A effective method to solve the problem is by the transformation of the non-uniform mesh to the uniform mesh. The algebraic transformation method is used to transform the fine mesh in the physical plane to the uniform mesh in the computational plane. The transformation is given:

$$x = x_q\left(1+\frac{\sinh[\tau(\varsigma-\delta)]}{\sinh(\tau\delta)}\right),\ \delta = \frac{1}{2\tau}\ln\left(\frac{1+(e^{\tau}-1)x_q}{1+(e^{-\tau}-1)x_q}\right) \quad (7)$$

In the transformation, x_q is the normal zone front coordinate, τ the stretching parameter which varies from zero to large values which generates the maximum refinement near x_q. Based on the coordinate transformation (7), the equations (1) and (2) in the physical plane can be transferred to the computational plane.

$$M\frac{\partial\psi}{\partial t} + A\frac{\partial\varsigma}{\partial x}\frac{\partial\psi}{\partial\varsigma} = G \quad (8)$$

$$\gamma C_{st}\frac{\partial T_{st}}{\partial t} = \frac{\partial\varsigma}{\partial x}\frac{\partial}{\partial\varsigma}\left(k_{st}\frac{\partial\varsigma}{\partial x}\frac{\partial T_{st}}{\partial\varsigma}\right) + Q_j + Q_d - \frac{Q_{st\text{-}cd} + Q_{st}}{A_{st}} \quad (9)$$

The transformation of partial derivation of coordinate is written as

$$\frac{\partial\varsigma}{\partial x} = \frac{\sinh(\delta\tau)}{\tau x_q\sqrt{1+\left(\frac{x}{x_q}-1\right)^2\sinh^2(\delta\tau)}} \text{ and}$$

$$\frac{\partial^2\varsigma}{\partial x^2} = \frac{(x_q - x)\sinh^3(\delta\tau)}{x_q^3\tau\left(1+\left(\frac{x}{x_q}-1\right)^2\sinh^2(\delta\tau)\right)^{\frac{3}{2}}} \quad (10)$$

The equations transferred to the computational plane can be discretized by the finite volume element on the staggered mesh in order to avoid the numerical instability. The standard boundary conditions are used for the equations [8]. The adiabatic boundary conditions are also imposed on the thermal conduction equation of superconducting strands. The integration with respect to the time is carried out with a standard θ-implicit finite difference approximation [9]. The nonlinear system equations are solved by the Global convergent method with compressible storage for the sparse Jacobi matrix [10].

The initial conditions can be determined by solving the steady-state equations of SHe. The temperature, pressure and flow velocity of SHe change with the length of the CICC. Generally, the CICC is connected with two constant SHe pressure reservoirs. The inlet temperature and outlet pressure can be specified. For the one-dimensional steady state equation of SHe, the temperature and pressure with respect to the length of the CICC are determined by the equations suggested by S.W.Van Sciver [11]. The equations are solved by a typical shooting method when the inlet temperature and outlet pressure are specified.

TABLE-I
THE PARAMETERS OF CICC

Superconductor	Nb_3Sn
Number. of Strands	486 (SC+ Cu)
Diame ter of strands	ϕ 0.8 mm
Cabling of pattern	3x3x3x3x6
Cooling perimeter of conduit	74.796 mm
RRR	100
Cross section area of conduit	242.69 mm^2
Cross section area of copper	149.82 mm^2
Superconductor cross section area	99.61 mm^2
He cross section area	140.46 mm^2
Cooling perimeter of strands	1.22 m
Operating current I_{opt}	35.16 kA
Hydraulic diameter	0.434 mm
Background field	7.35 T

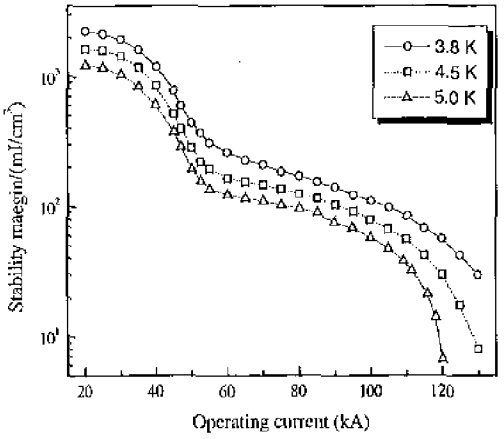

Fig.1 Stability margin vs operating current I_{opt} for different operating temperatures at t_d=10 ms, L_d=6m, B_m=7.35 T, pressure of 0.5 Mpa and mass flow rate of 0 g/s.

III. ANALYSIS OF THE STABILITY MARGIN

The main parameters of the CICC used in KSTAR are listed in Table-I [12]. The stability margin is calculated when the disturbance is located at the center of the CICC under the uniform field (B_m) of 7.35 T.

Fig.1 shows the stability margin versus operating current in various operating temperatures. The stability margin at operating temperature of 3.8 K is higher than that at 5K. This is because the critical current I_C and the current sharing temperature T_{sh} decrease with the increasing the operating temperature.

The influence of the mass flow rate of the SHe on the stability margin is illustrated in Fig.2. The stability margin becomes higher when the mass flow rate is fast. The limiting currents, where the stability margin falls sharply, increase for the mass flow rate changed from 0 g/s to 4 g/s. Fig.3 shows the stability margin versus operating current for the various magnetic fields. The stability margin at magnetic field of 9.4 T is much lower than that at 6.4 T. The limiting currents decrease monotonically with increasing the magnetic field [13].

Fig.4 illustrates the stability margin versus operating current for various disturbance duration times t_d. The stability margin is improved in well-cooled region when the disturbance duration is shorter. However, the disturbance duration time dependence of stability margin is reversed in ill-cooled region. The improvement of stability in the well-cooled region for the shorter disturbance duration can be explained as follows: (1) the shorter t_d corresponding to the high disturbance power. The disturbance is absorbed by the SHe and a strong SHe flow is induced as a results. The heat transfer coefficient is remarkably increased and the cooled condition of the conductor becomes better; (2) The minimum hot-spot temperature which induces a quench of the CICC becomes higher. The temperature gradient from the hot-spot to lower temperature region is so high that the longitudinal heat flow can suppress the hot-spot temperature rise. On the other hand, the heating induced flow is too small to enhance the heat transfer for the long distribution duration time.

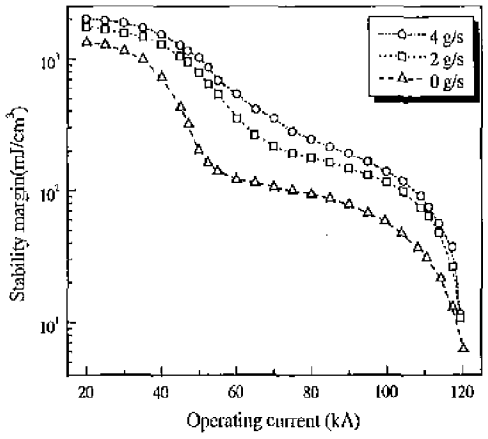

Fig.2 Stability margin vs operating current I_{opt} for different mass flow rates at t_d=10 ms, L_d=6m, B_m=7.35 T, inlet pressure of 0.5 MPa and inlet temperature of 4.5 K.

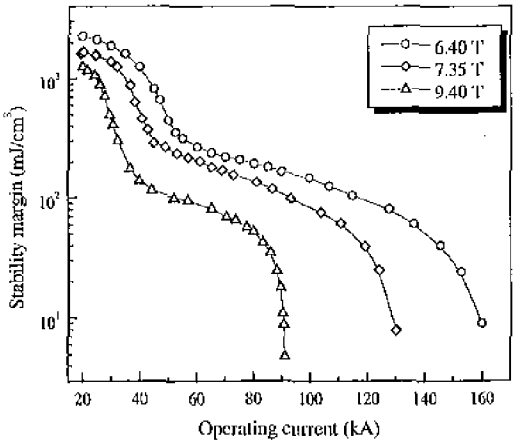

Fig.3 Stability margin vs operating current I_{opt} for different background fields at t_d=10 ms, L_d=6m, pressure of 0.5 Mpa, mass flow rate of 0 g/s and operating temperature of 4.5 K.

When the CICC quenches, the recovery of the CICC operated in the ill-cooled region is impossible. The conductor can only absorb relatively lower disturbance energy for short disturbance duration. The limiting current is increased with reducing the disturbance duration as shown in Fig.4. The stability margin with respect to disturbance length L_d is shown in Fig.5. The stability margin is increased when the disturbance length is shorter and its tendency becomes remarkable in the well-cooled region. The stability margin is generally determined at the beginning of disturbance within the tens of millisecond. The inertial and the friction force of the SHe can not be neglected for such a time scale. It is easy for the SHe to produce a stronger heating induced flow in shorter disturbance length. Therefore, the stability margin is limited by the available enthalpy ΔH of SHe. However, the SHe is difficult to expand for the longer disturbance length. The heat absorbed by the SHe causes its internal energy to increase. According to this, the stability margin is limited by the available internal energy ΔU.

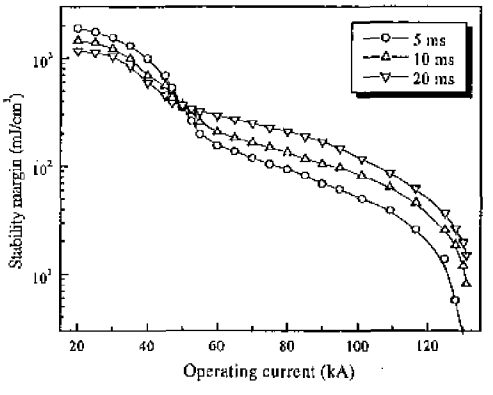

Fig.4 Stability margin vs operating current I_{opt} for various distribution duration times at L_d=6m, B_m=7.35 T, pressure of 0.5 MPa, mass flow rate of 0 g/s and operating temperature of 4.5 K.

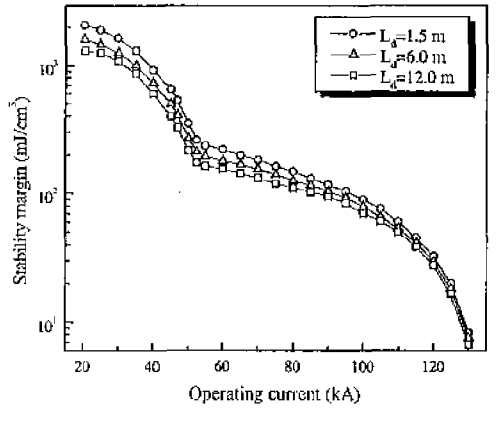

Fig.5 Stability margin vs operating current I_{opt} for various disturbance lengths at t_d=10 ms, B_m=7.35 T, pressure of 0.5 MPa, mass flow rate of 0 g/s and operating temperature of 4.5 K.

From the analysis of the stability margin with respect to the function of operating current of CICC in various cryogenic operating parameters and disturbances, the parameters can only influence on the amplitude of stability margin, but they cann't change the varying rule. Therefore, the shape of the curves is the same.

IV. Conclusions

The numerical simulation of the stability margin for the CICC has been performed by the numerical method. The time integration can be controlled by θ-implicit scheme. For the θ=1/2, the second-order time accuracy is obtained. The Global Convergence method is used to solve the equations with full-implicit time stepping scheme. The algebraic method is applied to transfer the fine mesh in the physics plane to uniform mesh in the computational plane. The stability margin increases for the fast mass flow, lower operating temperature and magnetic field. The limiting current decreases with increasing magnetic field. When the disturbance duration becomes shorter, the stability margin increases in the well-cooled region and its tendency reverses in the ill-cooled region.

References

[1] Jeol H. Schultz, "The KSTAR superconducting magnet system,", *KSTAR Design Point Definition File*, 1997.

[2] J.W.Lue, "Review of stability experiments on cable-in-conduit conductors," *Cryogenics*, Vol. 34, pp779-786, No.10, 1994.

[3] J.W.Lue, J.R.Miller, L.Dresner, "Stability of Cable-in-Conduit superconductors," *J.of Applied physics*, Vol.51, pp 772-783, No.1 1981.

[4] Q.Wang, S.Oh, K.Kang, C.Yoon ,K.Kim," Numerical analysis of stability margin and quench behavior of Cable-in-conduit NbTi conductors for KSTAR," *IEEE Transactions On Applied Superconductivity*, Vol. 9, pp620-624, No.3, 1999.

[5] C.Marinucci, CRPP/FT/CM/98-RB-01,1998.

[6] N.Koizumi, Y.Takashi, H.Tsuji, "Numerical model using an implicit finite difference algorithm for stability simulation of a cable-in-conduit superconductor," *Cryogenics*, Vol 36, pp 649-659, No.9, 1996.

[7] L.Bottura, A.Shajii, "On the numerical studies of quench in Cable-in-conduit conductors," *IEEE Transactions on Applied Superconductivity*, Vol.5, pp 495-498, No.2, 1998.

[8] A. Shajii, MIT PFC/RR-94-9, 1994.

[9] L.Bottura, " A numerical model for the simulation of quench in the ITER magnets," *J.of Computational Physics*, Vol.125, pp26-41, No.2, 1996.

[10] Willian H. Press, Saul A. Teukolsky, William T.Vetterling, Brian P.Flannery, *Numerical Recipes in Fortran*, Cambridge University Press, 1992

[11] S.W.Van Sciver, *Helium Cryogenics*, Plenum Press, New York, 1986.

[12] KSTAR superconducting Tokamak team, *KSTAR Magnet System Revier Files*,August, *1999*.

[13] L.Dresner, *Stability of Superconductors*, Plenum Press, New York, 1995.